Monthly Notices of the ROYAL ASTRONOMICAL SOCIETY

MNRAS **516,** 100–105 (2022) https://doi.org/10.1093/mnras/stac2194
Advance Access publication 2022 August 13

VLT/UVES observation of the outflow in quasar SDSS J1439-0106

Doyee Byun ,★ Nahum Arav and Andrew Walker
Virginia Tech, Blacksburg, Virginia, VA 24061, USA

Accepted 2022 July 26. Received 2022 July 22; in original form 2022 June 6

ABSTRACT

We analyse the VLT/UVES spectrum of the quasar SDSS J143907.5-010616.7, retrieved from the UVES Spectral Quasar Absorption Database. We identify two outflow systems in the spectrum: a mini broad absorption line (mini-BAL) system and a narrow absorption line (NAL) system. We measure the ionic column densities of the mini-BAL ($v = -1550\,\mathrm{km\ s^{-1}}$) outflow, which has excited state absorption troughs of Fe II. We determine that the electron number density $\log n_e = 3.4^{+0.1}_{-0.1}$, based on the ratios between the excited and ground state abundances of Fe II, and find the kinetic luminosity of the outflow to be $\lesssim$0.1 per cent of the quasar's Eddington luminosity, making it insufficient to contribute to AGN feedback.

Key words: galaxies: active – quasars: absorption lines – quasars: individual: SDSS J143907.5-010616.7.

1 INTRODUCTION

Quasar outflows are often found in the spectra of quasars ($\lesssim$40 per cent) as blueshifted absorption troughs relative to the rest frame of the quasars (Hewett & Foltz 2003; Dai, Shankar & Sivakoff 2008; Knigge et al. 2008). Often invoked as potential contributors to AGN feedback analysis of these outflows can provide us with insight into galaxy evolution (e.g. Silk & Rees 1998; Yuan et al. 2018; Vayner et al. 2021; He et al. 2022). The outflows must have a kinetic luminosity ($\dot{E}_\mathrm{k}$) of at least ∼0.5 per cent (Hopkins & Elvis 2010) or perhaps as much as ∼5 per cent (Scannapieco & Oh 2004) of the quasar's Eddington luminosity (L_Edd), depending on the theoretical model to be contributors of AGN feedback. Several outflows with sufficient $\dot{E}_\mathrm{k}$ have been found in past studies (e.g. Moe et al. 2009; Arav et al. 2013; Chamberlain, Arav & Benn 2015; Leighly et al. 2018; Xu et al. 2019; Miller et al. 2020a; Byun, Arav & Hall 2022; Choi et al. 2022).

Crucial to the process of finding a quasar outflow's kinetic luminosity is finding its mass flow rate ($\dot{M}$), which is dependent on its hydrogen column density (N_H), ionization parameter (U_H), and electron number density (n_e) (Borguet et al. 2012b). Analysis using this method has been conducted in the past (e.g. de Kool et al. 2001; Hamann et al. 2001; Xu et al. 2018; Arav et al. 2020; Walker et al., in preparation). The value of n_e can be found by calculating the ratios between the excited and resonance state column densities of ions (Arav et al. 2018). This paper presents the determination of $\dot{E}_\mathrm{k}$ of one of the outflow components of the quasar SDSS J143907.50-010616.7 (hereafter J1439-0106), based on the normalized VLT/UVES spectrum acquired from the Spectral Quasar Absorption Database (SQUAD) published by Murphy et al. (2019). Similar analysis using data from this data base has been conducted in previous studies (Byun et al. 2022; Byun et al., in preparation; Walker et al., in preparation).

The UVES data of J1439-0106 was collected as part of the programs 081.B-0285(A) and 083.B-0604(A), and has been added to the SQUAD data base complied by Murphy et al. (2019). From the normalized spectrum, we identify two distinct absorption outflow systems, which we label here as the mini broad absorption line (mini-BAL) system S1, and the narrow absorption line (NAL) system S2 of which we find S1 suitable for our analysis thanks to the presence of excited state absorption troughs.

This paper is structured as follows. Section 2 describes the observation of J1439-0106, as well as the method we used to retrieve its spectral data. Section 3 discusses the measurement of ionic column densities of S1, as well as the determination of N_H, U_H, and n_e. Section 4 shows the resulting calculation of $\dot{M}$ and $\dot{E}_\mathrm{k}$, as well as its ratio with L_Edd. Section 5 provides a discussion of these results, as well as a comparison with previous work. Section 6 summarizes and concludes the paper. We adopt a cosmology of $h = 0.696$, $\Omega_m = 0.286$, and $\Omega_\Lambda = 0.714$ (Bennett et al. 2014). We use the Python astronomy package Astropy (Astropy Collaboration et al. 2013, 2018) for cosmological calculations.

2 OBSERVATION AND DATA ACQUISITION

J1439-0106 (J2000: RA = 14:39:07.5, DEC = -01:06:16.7, $z = 1.819$) was observed with VLT/UVES on 2008 May 1, as part of the program 081.B-0285(A), and on 2009 April 16, as part of 083.B-0604(A), with minimal variability between the two epochs. The combined spectral data, covering wavelengths between 3284–9466 Å, was normalized by the quasar's continuum and emission, and added to the SQUAD data base by Murphy et al. (2019). The spectrum is shown in Fig. 1. The object was also observed in 2002 May 15, as part of the Sloan Digital Sky Survey (SDSS) (Abazajian et al, 2004), the spectrum of which we use to calibrate the flux shown in Fig. 1, as well as find the bolometric and Eddington luminosities of the quasar.

From the UVES spectrum, we identify two different absorption outflow systems, mini-BAL S1 ($v \approx -1550\,\mathrm{km\ s^{-1}}$), and NAL S2 ($v \approx -2750\,\mathrm{km\ s^{-1}}$). We focus on S1 in the analysis of this paper,

★ E-mail: dbyun@vt.edu

© 2022 The Author(s)
Published by Oxford University Press on behalf of Royal Astronomical Society

Downloaded from https://academic.oup.com/mnras/article/516/1/100/6665942 by Virginia Polytechnic Institute and State University - Main Library user on 21 June 2023

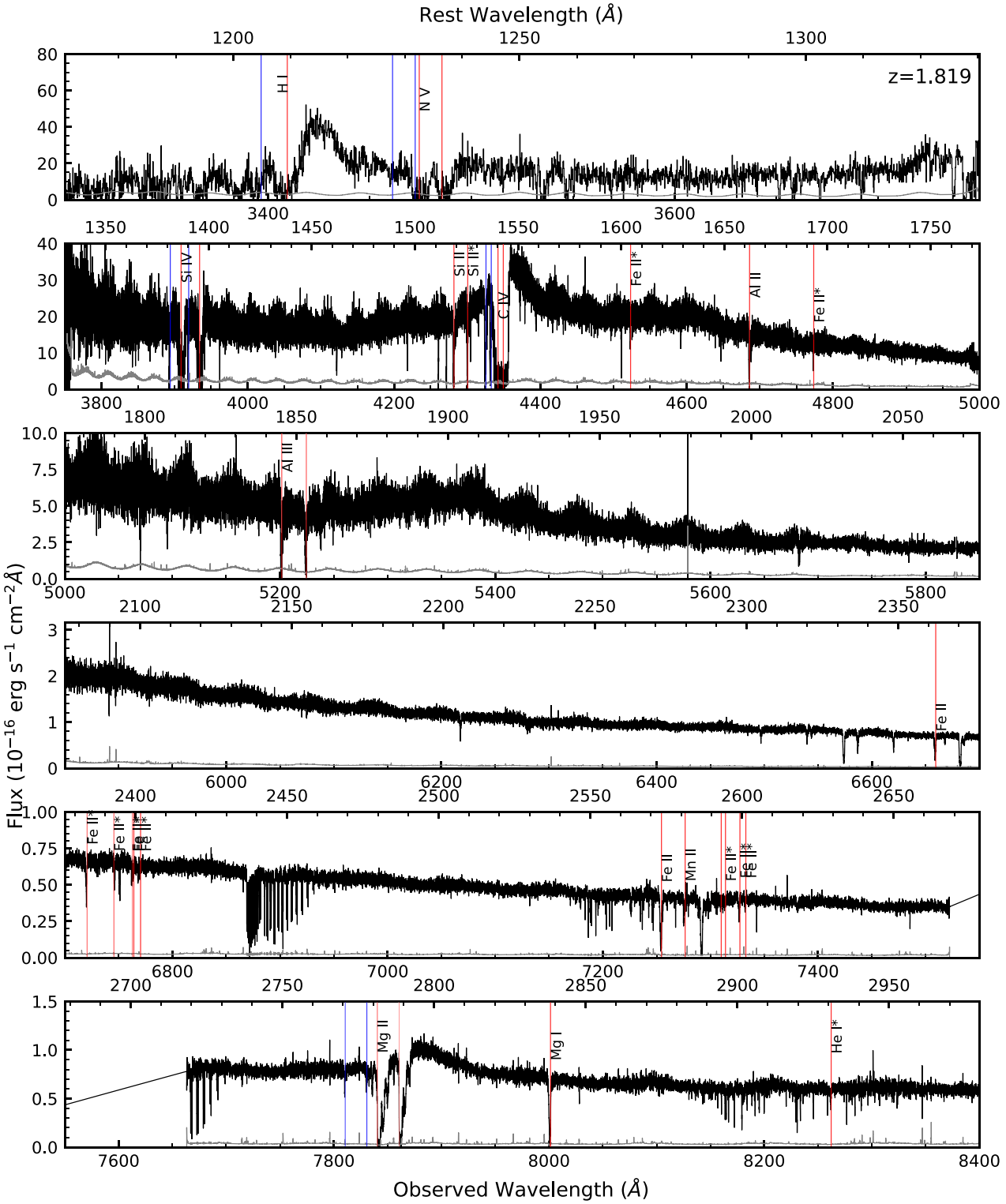

Figure 1. The UVES spectrum of J1439-0106. The normalized spectrum was multiplied by the continuum model by Murphy et al. (2019), and scaled to match the flux of the SDSS spectrum at observed wavelength 6500 Å. Red vertical lines mark the absorption features of S1, and the blue vertical lines mark the features of S2. While in S2, troughs of C IV, Si IV, Mg II, H I, and N V are detected, they are shallower and narrower than those of S1. The first panel has been binned by 10 pixels for clarity.

Downloaded from https://academic.oup.com/mnras/article/516/1/100/6665942 by Virginia Polytechnic Institute and State University - Main Library user on 21 June 2023

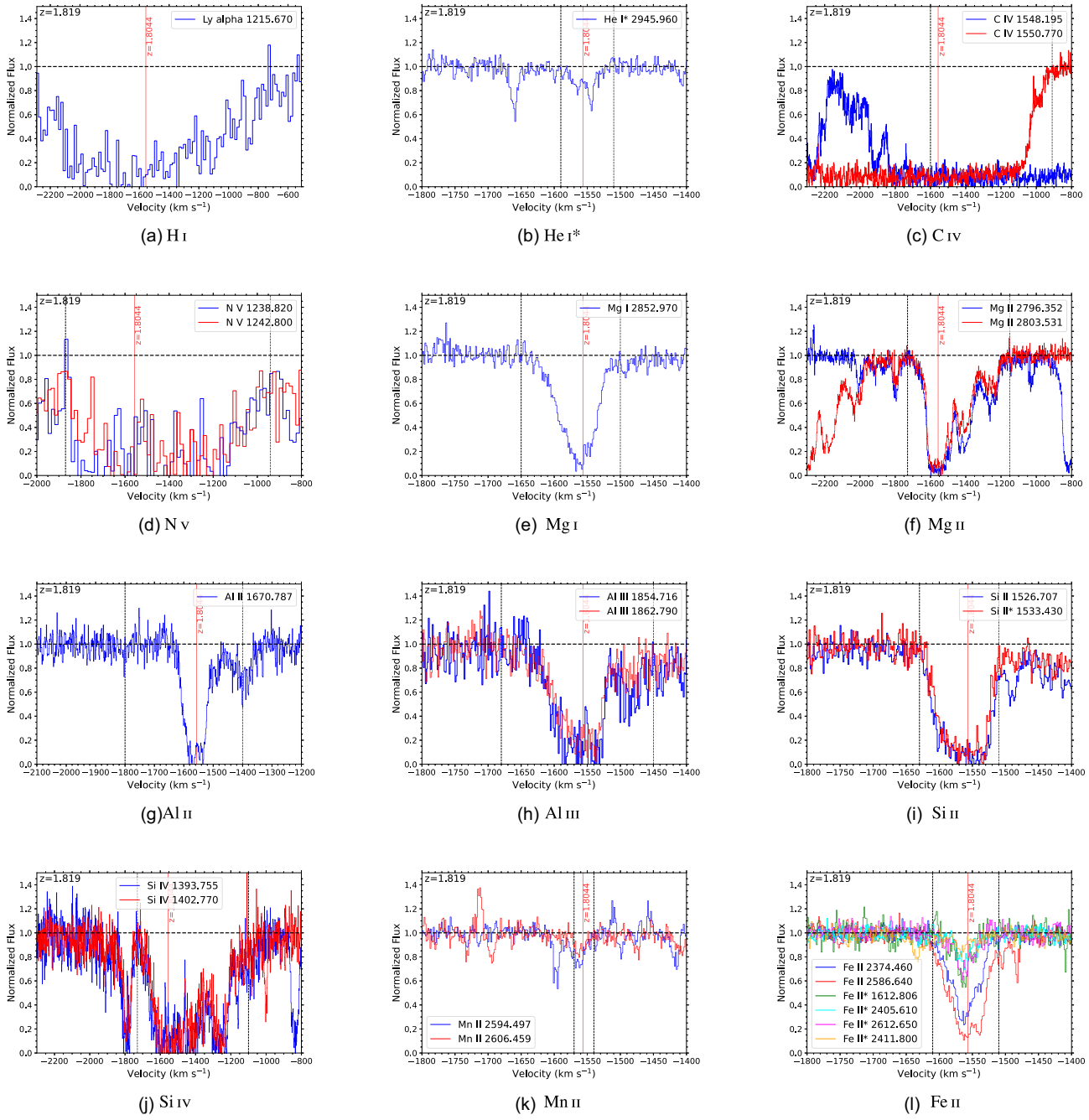

Figure 2. Absorption troughs of the outflow system S1 plotted in velocity space. The horizontal dashed line indicates the continuum level, while the vertical red line shows the velocity of S1. The vertical dotted lines show the integration range used to find the column densities.

as it shows troughs of several Fe II excited lines, allowing us to find the outflow distance from the source, and by extension, the mass flow rate.

3 ANALYSIS

3.1 Ionic column densities

Finding the ionic column densities ($N_{\rm ion}$) of S1 is crucial to determine the energetics parameters of the outflow system. In order to measure the column densities, we use the systemic redshift of the quasar to convert the spectrum from wavelength space to velocity space, as shown in Fig. 2. We then use two different methods to find the ionic column densities, assuming either an apparent optical depth (AOD) of a uniform outflow (Savage & Sembach 1991), or partial covering (PC) based on a velocity dependent covering factor (Barlow, Hamann & Sargent 1997; Arav et al. 1999a, b).

The AOD method and PC method have different advantages over one another with the PC method being particularly more helpful in finding more accurate column densities for ions with absorption doublets or multiplets, while the AOD method yields lower limits to the column densities (de Kool, Korista & Arav 2002; Arav et al. 2005; Edmonds et al. 2011; Borguet et al. 2012a). The differences

Downloaded from https://academic.oup.com/mnras/article/516/1/100/6665942 by Virginia Polytechnic Institute and State University - Main Library user on 21 June 2023

Table 1. J1439-0106 outflow column densities from UVES observations. The values are in units of 10^{12} cm^{-2}.

Troughs	AOD	PC	Adopted
	S1, $v = -1550$ kms^{-1}		
H I	1450^{+80}_{-40}		$>1450_{-290}$
He I*	100^{+6}_{-6}		$>100_{-20}$
C IV	3440^{+50}_{-40}		$>3440_{-690}$
N V	3370^{+220}_{-140}		$>3370_{-690}$
Mg I	$7.8^{+0.2}_{-0.2}$		$>8_{-1.6}$
Mg II	196^{+4}_{-3}	250^{+70}_{-4}	250^{+80}_{-50}
Al II	25^{+2}_{-1}		$>25_{-5}$
Al III	96^{+3}_{-3}		$>100_{-20}$
Si II total	720^{+30}_{-20}		$>720_{-100}$
Si II 0	410^{+25}_{-15}		
Si II*	310^{+15}_{-10}		
Si IV	850^{+40}_{-20}		$>850_{-170}$
Mn II	$2.7^{+0.3}_{-0.3}$	$2.8^{+0.2}_{-0.2}$	$2.8^{+0.6}_{-0.6}$
Fe II total			$>430_{-60}$
Fe II 0	230^{+4}_{-4}	270^{+5}_{-5}	270^{+50}_{-50}
Fe II* 385	16^{+3}_{-3}	21^{+3}_{-1}	21^{+5}_{-4}
Fe II* 668	14^{+4}_{-4}	18^{+6}_{-4}	18^{+7}_{-6}
Fe II* 862	7^{+1}_{-1}		$7^{+1.5}_{-1.6}$
Fe II* 977	$3.8^{+0.4}_{-0.3}$		$3.8^{+0.8}_{-0.8}$
Fe II* 1873	100^{+10}_{-10}	110^{+10}_{-10}	110^{+20}_{-20}

between the two methods is explained in further detail in Section 3.1 of Byun et al. (2022).

We choose our integration range for each ion based on the visibility of absorption troughs, as shown in Fig. 2. In cases the red and blue troughs of a doublet are blended (e.g. C IV), we choose a range in which the red and blue troughs are not overlapping in order to gain a lower limit of the column density. The measured column densities are shown in Table 1. Note that we add a 20 per cent error in quadrature to account for the uncertainty in the continuum model (Xu et al. 2018).

3.2 Photoionization analysis

With the ionic column densities found, we can use these measurements to find the hydrogen column density ($N_{\rm H}$) and ionization parameter ($U_{\rm H}$) of S1 (e.g. Xu et al. 2019; Miller et al. 2020a; Byun et al. 2022, Walker et al., in preparation). We use the spectral synthesis code Cloudy (Ferland et al. 2017, version c17.00) to create a grid of simulated models based on varying values of $N_{\rm H}$ and $U_{\rm H}$, using the spectral energy distribution (SED) of quasar HE0238-1904 (hereafter HE0238) (Arav et al. 2013). Via χ^2 analysis, we find the model with ionic column densities that best match the measured values, as shown in Fig. 3. We use two different grids based on metallicity values solar and super-solar ($Z = 4.68Z_{\odot}$ Ballero et al. 2008; Miller et al. 2020b) to find two different solutions, as previous studies show that the metallicities of outflows are between $Z_{\odot}$ and $5Z_{\odot}$ (e.g. Gabel, Arav & Kim 2006; Arav et al. 2007; Miller et al. 2020b). The values of $N_{\rm H}$ and $U_{\rm H}$ are shown in Table 2.

3.3 Electron number density

Finding the distance of the outflow from its source is crucial to finding the mass flow rate, and by extension, the kinetic luminosity. This is done by finding the electron number density (n_e), which is measured by taking the ratios between excited and ground state column densities of ions (e.g. Moe et al. 2009; Byun et al. 2022). The CHIANTI 9.0.1 Data base (Dere et al. 1997; Dere et al. 2019) models, the n_e dependent ratios between different energy states based on collisional excitation, and can be used to find the value of n_e from measured column densities. S1 shows absorption lines of five different excited states, as well as the ground state, of Fe II, and we find n_e by finding the ratios between these excited states and the resonance state (N(Fe II*)/N(Fe II)), as shown in Fig. 4. While we find troughs of Si II and Si II*, they are unreliable for finding n_e due to the saturation of the troughs (see plot i in Fig. 2). We find the weighted mean of the log n_e values measured using the different excited states via the linear model method described by Barlow (2003). This yields a value of $\log n_e = 3.4^{+0.1}_{-0.1}$.

4 RESULTS

The distance of the outflow from the quasar can be found based on the definition of the ionization parameter:

$$U_{\rm H} \equiv \frac{Q_{\rm H}}{4\pi R^2 n_{\rm H} c} \tag{1}$$

where $Q_{\rm H}$ is the emission rate of hydrogen ionizing photons, R is the distance from the source, c is the speed of light, and $n_{\rm H}$ is the hydrogen number density. Once we find $Q_{\rm H}$, we can use the values of $U_{\rm H}$ and n_e found in Section 3 to find R, as $n_e \approx 1.2\, n_{\rm H}$ in highly ionized plasma (Osterbrock & Ferland 2006).

We find the value of $Q_{\rm H}$ as follows, as per previous works (e.g. Miller et al. 2020a; Byun et al. 2022, Byun et al., in preparation; Walker et al., in preparation). We scale the SED of HE0238 to match the continuum flux of J1439-0106 at observed wavelength $\lambda = 6500$ Å, from the SDSS observation of 2002 May 15, ($F_\lambda = 8.49^{+0.64}_{-0.64} \times 10^{-17}$ erg s^{-1} cm^{-2} Å^{-1}). We then integrated over the SED for energies over 1 Ryd, resulting in $Q_{\rm H} = 5.3^{+0.4}_{-0.4} \times 10^{56}$ s^{-1}.

Once the distance is found, we can find the mass flow rate ($\dot{M}$) and kinetic luminosity ($\dot{E}_{\rm k}$) as shown in the following (Borguet et al. 2012a):

$$\dot{M} \simeq 4\pi \Omega R N_{\rm H} \mu m_p v \tag{2}$$

$$\dot{E}_{\rm k} \simeq \frac{1}{2}\dot{M} v^2, \tag{3}$$

where Ω is the fraction of the solid angle covered by the outflow, $\mu = 1.4$ is the molecular weight, m_p is the mass of a proton, and v is the outflow velocity. We assume $\Omega = 0.2$ based on ratio of quasars with C IV BALs reported by Hewett & Foltz (2003). When propagating the uncertainties of the parameters, we take into account the positive correlation between $U_{\rm H}$ and N_H in the photoionization solutions (see Fig. 3) to avoid overestimating our errors (see Walker et al. (in preparation) for a detailed explanation). The values found for $\dot{M}$ and $\dot{E}_{\rm k}$ are in Table 2.

5 DISCUSSION

5.1 AGN feedback contribution

In order to be a major contributor to AGN feedback, S1 needs to have a kinetic energy of at least ∼0.5 per cent (Hopkins & Elvis 2010) or perhaps as much as ∼5 per cent (Scannapieco & Oh 2004) of the quasar's Eddington luminosity ($L_{\rm Edd}$), depending on the theoretical model. To find $L_{\rm Edd}$, we follow the method by Byun et al. (2022),

Downloaded from https://academic.oup.com/mnras/article/516/1/100/6665942 by Virginia Polytechnic Institute and State University - Main Library user on 21 June 2023

Table 2. Physical properties of J1439-0106 outflow.

Solution	Solar	Super-solar
$\log(N_{\rm H})$ $[{\rm cm}^{-2}]$	$20.99^{+0.61}_{-0.59}$	$20.13^{+1.03}_{-0.71}$
$\log(U_{\rm H})$ [dex]	$-1.99^{+0.60}_{-0.58}$	$-2.44^{+0.85}_{-0.45}$
$\log(n_{\rm e})$ $[{\rm cm}^{-3}]$	$3.4^{+0.1}_{-0.1}$	$3.4^{+0.1}_{-0.1}$
Distance [pc]	2600^{+2500}_{-1300}	4400^{+3100}_{-2800}
$\dot{M}$ $[{\rm M}_\odot\ {\rm yr}^{-1}]$	110^{+120}_{-60}	30^{+80}_{-20}
$\dot{M}v$ $[10^{36}\ {\rm ergs\ cm}^{-1}]$	$1.1^{+1.2}_{-0.6}$	$0.27^{+0.82}_{-0.18}$
$\log(\dot{E}_K)$ $[{\rm erg\ s}^{-1}]$	$43.94^{+0.31}_{-0.32}$	$43.32^{+0.49}_{-0.61}$
$\dot{E}_K/L_{\rm Edd}$ [%]	$0.099^{+0.12}_{-0.05}$	$0.023^{+0.053}_{-0.018}$

finding the full width at half max (FWHM) of the Mg II emission in the SDSS spectrum, and using the Mg II-based equation by Bahk, Woo & Park (2019) to find the mass of the black hole. As there is Fe II emission in the region of Mg II emission, we use the Fe II template by Tsuzuki et al. (2006) and run a best-fitting algorithm to match the template to the spectrum, following Woo et al. (2018).

The resulting black hole mass is $M_{\rm BH} = 7.05^{+2.68}_{-2.03} \times 10^8 {\rm M}_\odot$ with a corresponding Eddington luminosity of $L_{\rm Edd} = 8.89^{+3.38}_{-2.56} \times 10^{46}$ erg s^{-1}. The Eddington ratio of the outflow ranges from $0.099^{+0.12}_{-0.05}$ per cent (for solar metallicity) to $0.023^{+0.053}_{-0.018}$ per cent (for super-solar metallicity), which is below the threshold for AGN feedback contribution.

5.2 Comparison with previous work

We have found the value of $n_{\rm H}$ of S1 based on the ratios between the column densities of excited state and resonance state Fe II. This has notably done by Korista et al. (2008) for the outflow of the quasar NVSS J235953-124148. The $\log n_e$ values from the different energy states in Fig. 4 are in agreement within ∼0.2 dex, which is comparable to the agreement shown in fig. 3 of Korista et al. (2008), showing that the ratios between Fe II energy states can be consistently used to probe the n_e value and the distance of an outflow from its source.

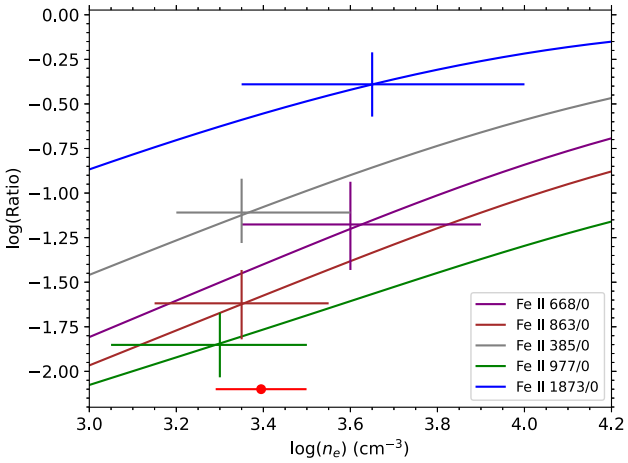

Figure 4. Log-log plot of the ratios between excited state Fe II and resonance state Fe II versus electron number density. The curves show the theoretical relationship between the ratios and n_e values, while the crosses show the measured ratios and their associated n_e. The red dot with error bars indicates the weighted mean of $\log n_e$. A temperature of 10 000K is assumed.

6 SUMMARY AND CONCLUSION

We have identified two outflow systems from the VLT/UVES spectrum of the quasar SDSS J1439-0106, the mini-BAL S1, and the NAL S2. After measuring the column densities of the ions identified in S1, we used these measurements to find the $N_{\rm H}$ and $U_{\rm H}$ values of S1 via photoionization analysis using models of both solar and super-solar metallicity (see Fig. 3).

With the abundance ratios between five different excited states of Fe II and the resonance state, we found the electron number density of

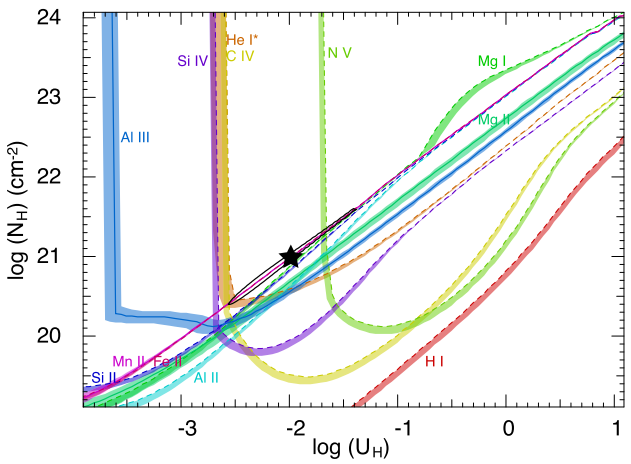

(a) Solar metallicity

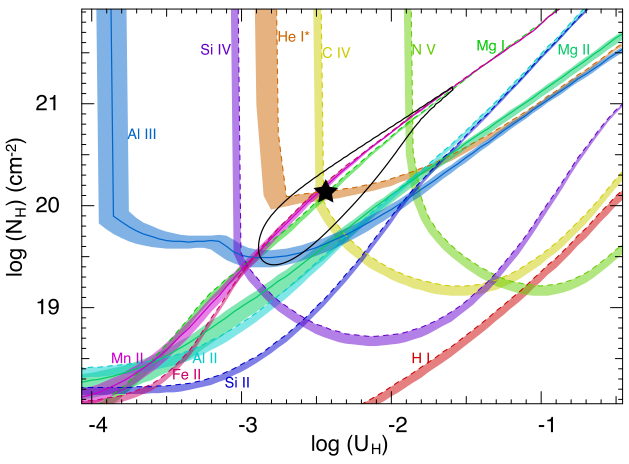

(b) Super-solar metallicity (see text)

Figure 3. Plots of $\log N_{\rm H}$ versus $\log U_{\rm H}$ based on the ionic column densities of S1. The coloured lines show the values of $N_{\rm H}$ and $U_{\rm H}$ allowed by the measured column density of each ion. Solid lines indicate measurements, while the dashed lines show lower limits from using the AOD method. The shaded bands attached to the lines represent the uncertainties in column density. The black stars indicate the solutions found via χ^2 analysis, and the black ellipses represent the 1σ error.

Downloaded from https://academic.oup.com/mnras/article/516/1/100/6665942 by Virginia Polytechnic Institute and State University - Main Library user on 21 June 2023

S1 (see Fig. 4). We have also found its distance from the quasar, the mass flow rate, and kinetic luminosity. Based on the ratio between the kinetic luminosity of S1 and the Eddington luminosity of the quasar, we conclude that it is insufficient for the outflow system to contribute to AGN feedback.

ACKNOWLEDGEMENTS

NA, DB, and AW acknowledge support from NSF grant AST 2106249, and NASA STScI grants AR-15786, AR-16600, and AR-16601.

DATA AVAILABILITY

The normalized UVES spectrum of J1439-0106 is part of the SQUAD data base made available by Murphy (2018) and described by Murphy et al. (2019). The SDSS spectrum is available in the SDSS data base (SDSS Data Release 2, Abazajian et al. 2004).

REFERENCES

Abazajian K. et al., 2004, ApJ, 128, 502
Arav N., Korista K. T., de Kool M., Junkkarinen V. T., Begelman M. C., 1999a, ApJ, 516, 27
Arav N., Becker R. H., Laurent-Muehleisen S. A., Gregg M. D., White R. L., Brotherton M. S., de Kool M., 1999b, ApJ, 524, 566
Arav N., Kaastra J., Kriss G. A., Korista K. T., Gabel J., Proga D., 2005, ApJ, 620, 665
Arav N. et al., 2007, ApJ, 658, 829
Arav N., Borguet B., Chamberlain C., Edmonds D., Danforth C., 2013, MNRAS, 436, 3286
Arav N., Liu G., Xu X., Stidham J., Benn C., Chamberlain C., 2018, ApJ, 857, 60
Arav N., Xu X., Miller T., Kriss G. A., Plesha R., 2020, ApJS, 247, 37
Astropy Collaboration, 2013, A&A, 558, A33
Astropy Collaboration, 2018, AJ, 156, 123
Bahk H., Woo J.-H., Park D., 2019, ApJ, 875, 50
Ballero S. K., Matteucci F., Ciotti L., Calura F., Padovani P., 2008, A&A, 478, 335
Barlow R., 2003, in Lyons L., Mount R., Reitmeyer R., eds, Proc. PHYSTAT 2003, Statistical Problems in Particle Physics, Astrophysics, and Cosmology. p. 250
Barlow T. A., Hamann F., Sargent W. L. W., 1997, in Arav N., Shlosman I., Weymann R. J., eds, ASP Conf. Ser. Vol. 128, Mass Ejection from Active Galactic Nuclei. Astron. Soc. Pac., San Francisco, p. 13
Bennett C. L., Larson D., Weiland J. L., Hinshaw G., 2014, ApJ, 794, 135
Borguet B. C. J., Edmonds D., Arav N., Dunn J., Kriss G. A., 2012a, ApJ, 751, 107
Borguet B. C. J., Edmonds D., Arav N., Benn C., Chamberlain C., 2012b, ApJ, 758, 69
Byun D., Arav N., Hall P. B., 2022, ApJ, 927, 176
Chamberlain C., Arav N., Benn C., 2015, MNRAS, 450, 1085
Choi H., Leighly K. M., Terndrup D. M., Dabbieri C., Gallagher S. C., Richards G. T., 2022, preprint (arXiv:2203.11964)
Dai X., Shankar F., Sivakoff G. R., 2008, ApJ, 672, 108
de Kool M., Arav N., Becker R. H., Gregg M. D., White R. L., Laurent-Muehleisen S. A., Price T., Korista K. T., 2001, ApJ, 548, 609
de Kool M., Korista K. T., Arav N., 2002, ApJ, 580, 54
Dere K. P., Landi E., Mason H. E., Monsignori Fossi B. C., Young P. R., 1997, A&AS, 125, 149
Dere K. P., Zanna G. D., Young P. R., Landi E., Sutherland R. S., 2019, ApJS, 241, 22
Edmonds D. et al., 2011, ApJ, 739, 7
Ferland G. J. et al., 2017, RMxAA, 53, 385
Gabel J. R., Arav N., Kim T.-S., 2006, ApJ, 646, 742
Hamann F. W., Barlow T. A., Chaffee F. C., Foltz C. B., Weymann R. J., 2001, ApJ, 550, 142
He Z. et al., 2022, Science Adv., 8, eabk3291
Hewett P. C., Foltz C. B., 2003, AJ, 125, 1784
Hopkins P. F., Elvis M., 2010, MNRAS, 401, 7
Knigge C., Scaringi S., Goad M. R., Cottis C. E., 2008, MNRAS, 386, 1426
Korista K. T., Bautista M. A., Arav N., Moe M., Costantini E., Benn C., 2008, ApJ, 688, 108
Leighly K. M., Terndrup D. M., Gallagher S. C., Richards G. T., Dietrich M., 2018, ApJ, 866, 7
Miller T. R., Arav N., Xu X., Kriss G. A., Plesha R. J., 2020a, ApJS, 247, 39
Miller T. R., Arav N., Xu X., Kriss G. A., Plesha R. J., 2020b, ApJS, 247, 41
Moe M., Arav N., Bautista M. A., Korista K. T., 2009, ApJ, 706, 525
Murphy M. T., Kacprzak G. G., Savorgnan G. A., Carswell R. F., 2019, MNRAS, 482, 3458
Murphy M., 2018, MTMurphy77/UVES_SQUAD_DR1: First data release of the UVES Spectral Quasar Absorption Database (SQUAD). Zenodo, available at https://doi.org/10.5281/zenodo.1463251
Osterbrock D. E., Ferland G. J., 2006, Astrophysics of gaseous nebulae and active galactic nuclei, 2nd edn. University Science Books, Sausalito
Savage B. D., Sembach K. R., 1991, ApJ, 379, 245
Scannapieco E., Oh S. P., 2004, ApJ, 608, 62
Silk J., Rees M. J., 1998, A&A, 331, L1
Tsuzuki Y., Kawara K., Yoshii Y., Oyabu S., Tanabé T., Matsuoka Y., 2006, ApJ, 650, 57
Vayner A. et al., 2021, ApJ, 919, 122
Woo J.-H., Le H. A. N., Karouzos M., Park D., Park D., Malkan M. A., Treu T., Bennert V. N., 2018, ApJ, 859, 138
Xu X., Arav N., Miller T., Benn C., 2018, ApJ, 858, 39
Xu X., Arav N., Miller T., Benn C., 2019, ApJ, 876, 105
Yuan F., Yoon D., Li Y.-P., Gan Z.-M., Ho L. C., Guo F., 2018, ApJ, 857, 121

This paper has been typeset from a TEX/LATEX file prepared by the author.

Downloaded from https://academic.oup.com/mnras/article/516/1/100/6665942 by Virginia Polytechnic Institute and State University - Main Library user on 21 June 2023